


Article

Aerodynamics of High-Speed Trains with Respect to Ground Simulation

Dennis Weidner ^{1,*} , Daniel Stoll ², Timo Kuthada ² and Andreas Wagner ¹

¹ Institute of Automotive Engineering (IFS), University of Stuttgart, 70569 Stuttgart, Germany; andreas.wagner@ifs.uni-stuttgart.de

² Research Institute for Automotive Engineering and Vehicle Powertrain Systems Stuttgart (FKFS), 70569 Stuttgart, Germany; daniel.stoll@fkfs.de (D.S.); timo.kuthada@fkfs.de (T.K.)

* Correspondence: dennis.weidner@ifs.uni-stuttgart.de

Abstract: Wind tunnel testing is commonly used to assess and optimize the aerodynamic characteristics of high-speed trains. The train model is usually mounted above a static ground plane, but a moving ground is necessary for the correct representation of the relative motion between train and ground. This study focuses on the effect of the applied ground simulation on the aerodynamics of a high-speed train. Wind tunnel tests using a stationary and a moving ground were carried out using a 1:20 scale model of a high-speed train's first car. Numerical simulations for two moving ground configurations are created, and the simulation setup is validated using surface pressure measurements from the wind tunnel tests. It is shown that the ground simulation has a significant effect on the drag in the considered yaw angle range. Additionally, the change in drag due to bogie fairings is evaluated and an impact of the applied ground simulation on the drag reduction is observed. The drag reduction of front and rear bogie fairings is valued similarly using a static ground, however on a moving ground the drag reduction of front bogie fairings is significantly increased. Good agreement between simulations and experiments is achieved.



Citation: Weidner, D.; Stoll, D.; Kuthada, T.; Wagner, A.

Aerodynamics of High-Speed Trains with Respect to Ground Simulation.

Fluids **2022**, *7*, 228. <https://doi.org/10.3390/fluids7070228>

Academic Editors: Mehrdad Massoudi, Christian Navid Nayeri, Sinisa Krajinovic and Iraj Mortazavi

Received: 7 June 2022

Accepted: 30 June 2022

Published: 5 July 2022

Publisher's Note: MDPI stays neutral with regard to jurisdictional claims in published maps and institutional affiliations.



Copyright: © 2022 by the authors. Licensee MDPI, Basel, Switzerland. This article is an open access article distributed under the terms and conditions of the Creative Commons Attribution (CC BY) license (<https://creativecommons.org/licenses/by/4.0/>).

Keywords: high-speed train; wind tunnel; ground simulation; bogie fairings

1. Introduction

The development of high-speed trains necessitates a thorough investigation of their aerodynamic performance. In addition to drag optimizations to reduce energy requirements, the stability in crosswind conditions, the induced flow in the vicinity of the train (slipstream velocities) and other aerodynamic aspects have to be considered.

Three tools are commonly used to assess the aerodynamic performance of high-speed trains: full-scale tests, tests at model scale and numerical simulations. Especially early on in the development process, model scale testing and numerical simulations are invaluable as cost-effective development environments. For model scale experiments, there are two common approaches, namely moving model testing and wind tunnel testing. With moving model testing, longer train models can be investigated, and the relative motion between train and ground is described correctly. Drawbacks of moving model testing are the requirement for unique testing facilities, and equipping the model for accurate force measurements is difficult. They are best suited for trackside measurements including measuring slipstream velocities, nose pressures and trackside structure loading [1]. Drag evaluations are usually restricted to cases where wind tunnel measurements are not possible, e.g., for long train models [2].

On the contrary, wind tunnel tests allow fast, reliable and repeatable measurements of aerodynamic forces. Their application is mainly for drag and crosswind sensitivity studies and limited to short train models. During wind tunnel tests, the model is normally mounted above a static ground plane, and thus the relative motion between train and ground is not modeled. As a consequence, a boundary layer grows along the ground plane, resulting

in unrealistic flow conditions underneath the train. Several studies using computational fluid dynamics (CFD) have analyzed the importance of a moving ground for drag and lift prediction.

In [3], Xia et al. used CFD to investigate a three car train model with different ground simulations. While the drag of the first car decreased by only four drag counts (one drag count: $\Delta c_D = 0.001$) when switching from a full moving ground to a static ground, the total drag of the three car train dropped by 6.4%. Additionally, the lift increased significantly, especially on the head car. They concluded that a moving ground is important for underbody investigations. Xia et al. also studied different moving ground conditions, where only part of the ground is moving akin to belts in automotive wind tunnels. They showed that using only a narrow belt between the wheels results in significant deviations from the full moving ground, whereas with a sufficiently wide belt these deviations are negligible.

Zhang et al. [4] also used a three car train model. They simulated using a stationary ground and a moving ground and assessed how rotating wheels affect the moving ground results. The difference in drag between moving and static ground for the first car was only two drag counts, but the overall drag was 6% higher using the moving ground. The effect of rotating wheels was small (three drag counts total). Large parts of the drag increases using the moving ground were caused on the bogies, again highlighting the need for a moving ground in this region.

In contrast to the previous two studies, Niu et al. [5] simulated the actual train movement instead of applying a moving ground boundary condition, thus replicating a moving model test. The moving head car's drag was 10% smaller than the stationary head car's drag. Significant pressure and velocity differences were observed along the underbody.

While multiple studies using CFD are available, experimental results using a moving ground are scarce. Baker and Brockie [6] analyzed wind tunnel results using moving and stationary grounds with the aim of extrapolating the full scale drag for journey time calculations, where accurate absolute drag values are necessary. They concluded that the ground simulation produces drag differences of around 10%, while the uncertainty of extrapolating to full-scale led to differences of up to 30% of the measured full scale drag. Thus, the extrapolation error is larger than the error caused by using a static ground, and a moving ground may not be necessary for such applications.

Kwon et al. [7] and Kwon et al. [8] published results of wind tunnel tests using different ground simulations. In [7], a high-speed train model was tested in two different wind tunnels, one using a moving belt and the other the usual static ground plane. They concluded that for evaluating drag reduction measures, the static ground plane is sufficient, while for absolute drag measurements, a moving ground is necessary. The drag of the three car train model was decreased by about 12% in the static ground tests. In [8], Kwon et al. tested two train models with different lengths and nose shapes in the same two wind tunnels with additional tests using a tangential blowing system in a third wind tunnel. The conclusions remained the same, adding that a tangential blowing system can be an alternative to a moving belt system.

The aim of the following study is to provide additional experimental results, using the same wind tunnel with both a moving and stationary ground and a standardized train model. The focus is not only on absolute drag values, but also on the importance for geometry changes. With increasing train speeds and energy costs, even small drag optimizations of high-speed trains are important, and thus need to be predicted accurately during development. At a speed of 300 km/h the aerodynamic drag accounts for about 75% of the driving resistance of a modern high-speed train on open, flat ground (using the "High Speed 300" reference data from [9]). This proportion is increasing rapidly with even higher train velocities. Bogie fairings as a drag reduction measure are slowly adopted in new high-speed trains across the world and the flow around them is affected by the underbody flow, which makes them ideal for this study. Bogie fairings offer a significant potential for drag reduction. For instance, Wang et al. [10] simulated the drag reductions

due to bogie fairings on a three car train. Using bogie fairings, the drag of the head car decreased by about 22% compared to the original model. The total drag of the three car model shrank by about 13%. The extensive experimental results are used to validate a CFD simulation setup. Lastly, the bogie fairings are simulated and compared to the wind tunnel tests.

2. Materials and Methods

Prior to this study, a 1:20 scale model of a high-speed train was built. It is based on the simplified ICE 3 reference geometry of the crosswind assessment standard EN 14067-6 [11]. The model consists of the first car and a downstream body, separated by a 5 mm gap to ensure that no force is transferred between the bodies. The model features a modular design to allow for geometry changes and easy access to any measurement equipment located inside the model. The segments were 3D printed, sanded, filled and finally painted to ensure a smooth surface finish. Then, 125 pressure taps were drilled into the model, with most of them located on the train nose (Figure 1). The model scale and length was chosen due to the size of the wind tunnel's test section and length of the central belt of its five-belt system (called centerbelt). Train models with additional train cars would need to be at a significantly smaller scale, resulting in difficulties to reach sufficiently high Reynolds numbers.

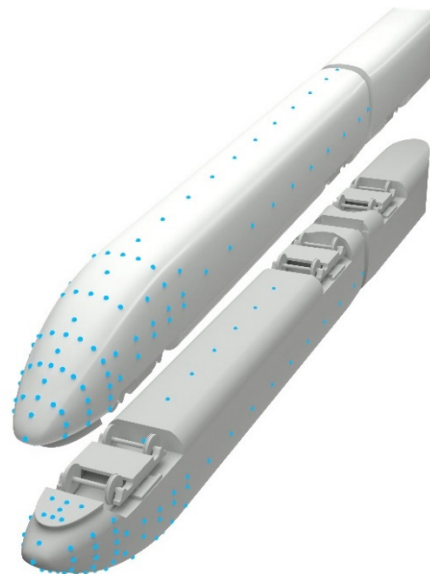


Figure 1. Locations of pressure taps on the model.

It is expected that the moving ground has a more significant impact on geometry changes made on a train's underbody than changes made higher up. As the underbody of the reference geometry is already smooth, bogie fairings were chosen as a design change to evaluate the influence of the ground simulation. The height of the bogie fairings is so that about two thirds of the front and rear bogie cutouts are covered (Figure 2). For the wind tunnel tests, the bogie fairings were again 3D printed and taped to the model.



Figure 2. Geometry of bogie fairings (D: height of the bogie cutout).

All wind tunnel measurements were carried out in the model scale wind tunnel of the Institute of Automotive Engineering (IFS) of the University of Stuttgart. It is a closed circuit wind tunnel with an open test section and its nozzle is 1.575 m wide and 1.05 m tall. The

ground simulation system consists of a five-belt system, a boundary layer pre-suction and tangential blowing in front of the 1.70 m long and 0.25 m wide center belt. For comparison, the first car's width is 0.148 m (59% of the centerbelt width) and its length is 1.301 m (77% of the centerbelt length). As the four wheel rotating units are connected to the wind tunnel balance, they could affect lift measurements and were therefore removed for this study. Wind speeds of up to 80 m/s are possible, however the wind speed in this study was 50 m/s. The resulting Reynolds number is about 5×10^5 (using a characteristic length $L = 0.15$ m) and thus in the range of constant pressure drag as recommended in [12]. Prior measurements with wind speeds ranging between 80 km/h and 270 km/h supported this recommendation. Forces and moments were measured using the wind tunnel's dynamic underfloor balance. Multiple runs were repeated once and on all occasions the drag coefficients of both runs were within one drag count. Further information about the flow quality, measurement equipment and control systems of the wind tunnel are published in [13].

As the centerbelt is used as the moving ground, the model is positioned according to the true flat ground configuration, as defined in [11]. Thus, the top of rail plane is 11.75 mm (235 mm full-scale) above the moving ground (Figure 3).



Figure 3. A 1:20 scale model in the IFS model scale wind tunnel of the University of Stuttgart, positioned according to the true flat ground configuration.

During the moving ground (MG) measurements, the full ground simulation was used, i.e., the centerbelt, boundary layer pre-suction and tangential blowing were switched on. For the static ground (SG) measurements, all ground simulation systems were turned off. In this case, the boundary layer thickness at the turntable center in the empty test section is about 40 mm [13]. This is still below the 30% of the model height threshold set out in EN 14067-6. Consequently, measurements using the static ground would be valid for crosswind assessments without any need for additional measures to reduce the boundary layer thickness of the incoming flow.

To measure the forces acting on the model, it is connected by two steel crossbeams to four vertical struts. The struts are connected to the wind tunnel's underfloor balance (Figure 4a). Similar struts are commonly used in the wind tunnel with 1:4 scale road vehicles. The aerodynamic forces on the struts and crossbeams were quantified by additional measurements where the model was held with two rods by the wind tunnel's model manipulator and thus, only the crossbeams and struts were connected to the underfloor balance (Figure 4b). Measurements with wind speed between 80 km/h and 270 km/h confirmed that the drag of the crossbeams and struts is Reynolds number independent in the considered range ($2 \times 10^5 < Re < 7 \times 10^5$). Especially for measurements at higher yaw angles, the interference effects between model support and train model are not captured using this method, but they were assumed small compared to the forces acting on the train model.

(a) Model, crossbeams and struts on balance



(b) Crossbeams and struts on balance model supported by manipulator



Figure 4. Model supports: (a) Model, crossbeams and struts are connected to the underfloor balance, (b) only the crossbeams and struts are on the balance, the train car model is supported by the wind tunnel’s manipulator.

Four Pressure Systems ESP-32HD pressure scanners were used for the surface pressure measurements. Their pressure range is about ± 7000 Pa, and the static accuracy is within $\pm 0.10\%$ FS. The pressure scanners were positioned inside the first car and connected to an external Pressure Systems DTC Initium data acquisition system. Pressures were sampled at 10 Hz for 30 s and subsequently time-averaged. All 125 pressures were measured simultaneously. To enable comparisons between measurements using different ground configurations as well as between experiments and simulations, the time-averaged pressures are corrected using the corresponding static pressure gradient of the empty test section. The pressure gradients with all ground simulation systems enabled as well as with all systems disabled are published in [13].

For the fluid simulations PowerFLOW 5.5b, a CFD package using the Lattice-Boltzmann-Method (LBM), was employed. The LBM is based on the mesoscopic kinetic theory. In contrast to the microscopic kinetic theory where particle motions are tracked, the mesoscopic kinetic theory involves tracking particle distributions [14]. The Boltzmann equation (Equation (1)) describes the evolution of the particle distribution function $f(x, v, t)$, with position x , particle velocity v , time t and the collision operator $\Omega(f)$. Macroscopic variables like density and velocity are moments of the particle distribution function. The left side of Equation (1) is the advection of the particle distribution function and the right side represents the redistribution of the particle distribution function due to collisions [14]. The collision operator in its simplest form is the Bhatnagar–Gross–Krook (BGK) collision operator (Equation (2)) with the relaxation time constant τ and the equilibrium distribution f^{eq} .

$$\frac{df}{dt} + v \frac{df}{dx} = \Omega(f) \tag{1}$$

$$\Omega(f) = -\frac{1}{\tau}(f - f^{eq}) \tag{2}$$

PowerFLOW uses the D3Q19 model (three spatial dimensions, 19 discrete velocities) for discretizing the Boltzmann equation on a lattice. The discretized form using the BGK collision operator is given as Equation (3) with discrete velocities c_i and time step Δt . Interactions between the fluid flow and surfaces are calculated using a volumetric boundary scheme [15]. At each facet particle bounce-back (no-slip), reflection (slip) or a combination of bounce-back and reflection (wall functions) processes occur [15].

$$f_i(x + c_i \Delta t, t + \Delta t) - f_i(x, t) = -\frac{1}{\tau} \left[f_i(x, t) - f_i^{eq}(x, t) \right] \tag{3}$$

Simulations are inherently transient and turbulence is modeled with the very large eddy simulation (VLES) approach. This approach is similar to hybrid Reynolds Averaged Navier–Stokes (RANS)—large eddy simulation (LES) turbulence modeling of finite volume Navier–Stokes based solvers. In PowerFLOW, large scale turbulence is resolved by the voxel grid (cells of the lattice are called voxels), whereas small scale turbulence is modeled by a modified Renormalization Group (RNG) k - ϵ turbulence model. The turbulence is represented in the BGK collision operator by adjusting the relaxation time scale τ to τ_{eff} as given in Equation (4) [15–17]. In Equation (4), T is the temperature, $\eta = k|S|/\epsilon$ the local strain parameter with the magnitude of the strain tensor $|S|$ and C_μ is a model coefficient ($C_\mu = 0.085$). The turbulent kinetic energy k is given in Equation (5) and the turbulent dissipation ϵ is calculated using Equation (6) [15–17]. ρ is the density, ν_0 is the molecular viscosity, ν_T is the eddy viscosity and τ_{ij} is the stress tensor. $C_{\epsilon 1} = 1.42$, $C_{\epsilon 2} = 1.68$, $\sigma_{k0} = \sigma_{kT} = \sigma_{\epsilon 0} = \sigma_{\epsilon T} = 0.719$, $\eta_0 = 4.38$ and $\beta = 0.012$ are model coefficients [17]. For high Reynolds number flows, e.g., flows around vehicles, wall functions are used [15].

$$\tau_{eff} = \tau + C_\mu \frac{k^2/\epsilon}{T(1 + \eta^2)^{1/2}} \tag{4}$$

$$\rho \frac{\partial k}{\partial t} + \rho v \cdot \nabla k = \frac{\partial}{\partial x_j} \left[\left(\frac{\rho \nu_0}{\sigma_{k0}} + \frac{\rho \nu_T}{\sigma_{kT}} \right) \frac{\partial k}{\partial x_j} \right] + \tau_{ij} S_{ij} - \rho \epsilon \tag{5}$$

$$\begin{aligned} \rho \frac{\partial \epsilon}{\partial t} + \rho v \cdot \nabla \epsilon &= \frac{\partial}{\partial x_j} \left[\left(\frac{\rho \nu_0}{\sigma_{\epsilon 0}} + \frac{\rho \nu_T}{\sigma_{\epsilon T}} \right) \frac{\partial \epsilon}{\partial x_j} \right] + C_{\epsilon 1} \frac{\epsilon}{k} \tau_{ij} S_{ij} \\ &\quad - \left[C_{\epsilon 2} + C_\mu \frac{\eta^3(1-\eta/\eta_0)}{1+\beta\eta^3} \right] \rho \frac{\epsilon^2}{k} \end{aligned} \tag{6}$$

The simulation was built using the same train geometry at 1:20 scale, also maintaining the gap between first car and downstream body. Instead of replicating the wind tunnel geometry, an idealized setup was employed: The model support was omitted and the simulation volume was significantly larger than the wind tunnel test section, resulting in a blockage of below 0.1% at 0° yaw. The idealized setup approach was chosen for its simplicity and to avoid introducing additional modeling errors that might be difficult to quantify (e.g., modeling of the boundary layer pre-suction). As the wind tunnel pressure measurements are corrected using the wind tunnel’s pressure gradient, the comparison of the pressure measurements and the simulations are valid.

The inlet velocity is set to 50 m/s (same as in the experiment) and the outlet is a zero pressure outlet. The walls of the simulation domain are frictionless walls, whereas two different approaches were used for the ground (Figure 5): In the first case, the complete ground surface is modeled as a moving wall, with the velocity set to the wind speed (Figure 5a). The second approach segments the ground in multiple section (Figure 5b): Firstly, a moving wall section sized and positioned like the centerbelt in the wind tunnel. The surface roughness of this centerbelt section is matched to the roughness of the wind tunnel’s centerbelt. Secondly, segments either side and downstream of the centerbelt are sized according to the test section dimensions. These segments are treated as no-slip walls. The remaining ground surfaces are slip walls, thus avoiding a boundary layer upstream of the centerbelt. The simulations are run for 0.5 s of physical time and averaged over the last 0.3 s.

The simulation domain is refined using multiple refinement regions. A general refinement box (voxel size 8 mm) extends about 15 train heights upstream of the model and 25 train heights downstream. It is 768 mm (96 local voxels) wide and 512 mm (64 local voxels) tall. The term local voxels refers to the number of voxels with the voxel size of the respective refinement region, i.e., 96 voxels of voxel size 8 mm. The far field is then constructed using subsequently coarser boxes (Figure 6a).

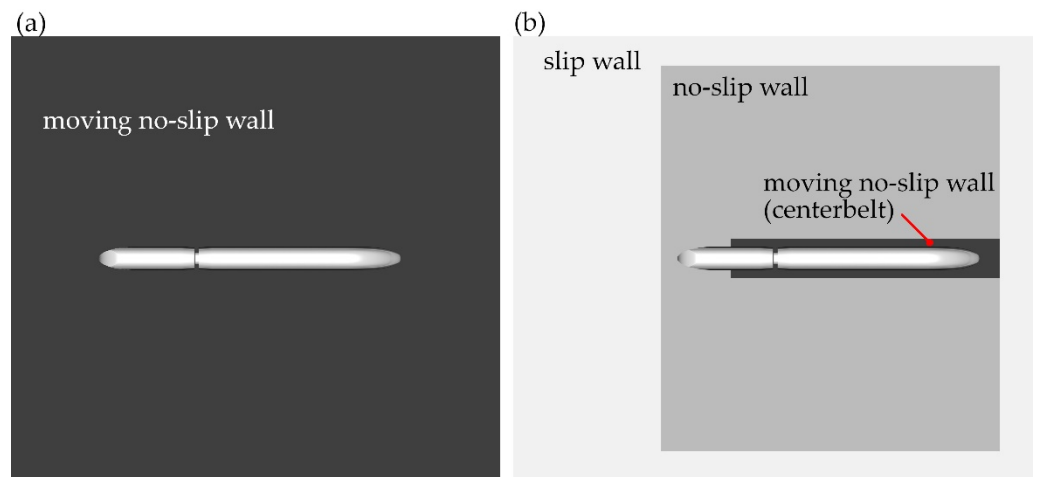


Figure 5. Ground boundary conditions: (a) full moving ground, (b) moving centerbelt.

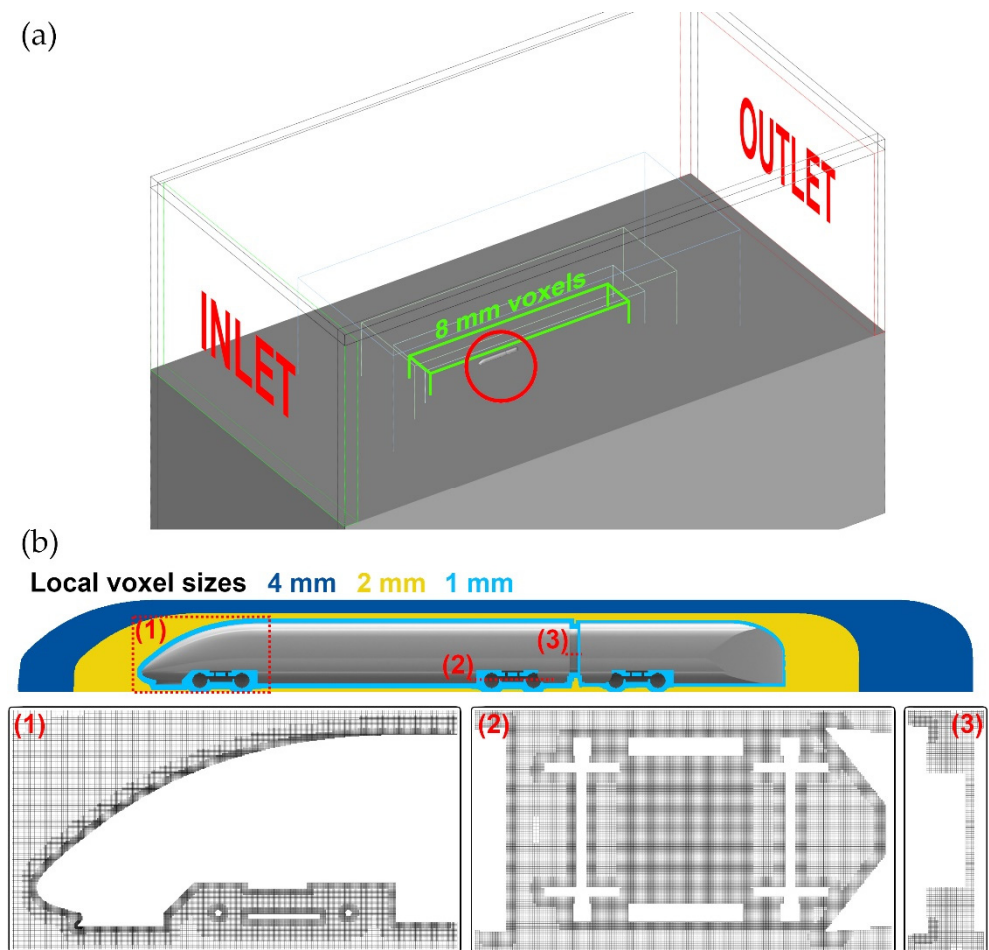


Figure 6. (a) Simulation domain, refinement box with 8 mm local voxel size highlighted, (b) extents of refinement regions with local voxel sizes of 4 mm, 2 mm and 1 mm and voxel grids for the train nose (1), around the rear bogie (2) and at the inter-car gap (3).

Near the surface of the train model additional refinement regions are employed, of which three are shown in Figure 6b. A 15 mm offset (local voxel size: 1 mm) encloses all train surfaces. To resolve the flow around the train two additional volume refinements are used: Firstly, a 40 mm (20 local voxels) offset that is extended 200 mm in front of the train

model and 250 mm behind the downstream body. Secondly, an 80 mm (20 local voxels) offset that extends 350 mm in front of the model and 600 mm behind the downstream body.

Select regions are further refined. The train nose up to the constant cross section of the car body, the bogies and the sharp edges of the bogie cutouts and inter-car gap are refined with a 7.5 mm offset of local voxel size 0.5 mm (Figure 6b (1–3)). The front lip (cowcatcher) is refined with a 2.5 mm offset of local voxel size 0.25 mm (Figure 6b (1)). These refinements result in a wall y^+ of around 30 on the train nose and around 60 along the remaining train surfaces for a wind speed of 50 m/s.

A grid sensitivity study was performed by scaling the voxel sizes. Three different grid sizes were investigated. The edge length of the smallest voxels varied between 0.25 mm (fine), 0.3125 mm (medium) and 0.375 mm (coarse). All other voxel sizes are scaled accordingly, but the simulation domain dimensions were unchanged. The surface pressure profiles for three sections are shown in Figure 7. For the first section, differences in pressure between the three grids can be observed primarily on the underbody. The lowest pressures near the 0° angle indicator occur on the finest grid. Analysis of the force development profiles along the head car showed some differences near the front bogie, and thus in a region strongly influenced by the upstream underbody flow. For the sections downstream of the front bogie cutout and in front of the rear bogie cutout, deviations between the fine and medium grids are small. The underbody surface pressure (-30° to 30°) is higher on the coarse grid. All subsequent results were obtained using the fine grid.

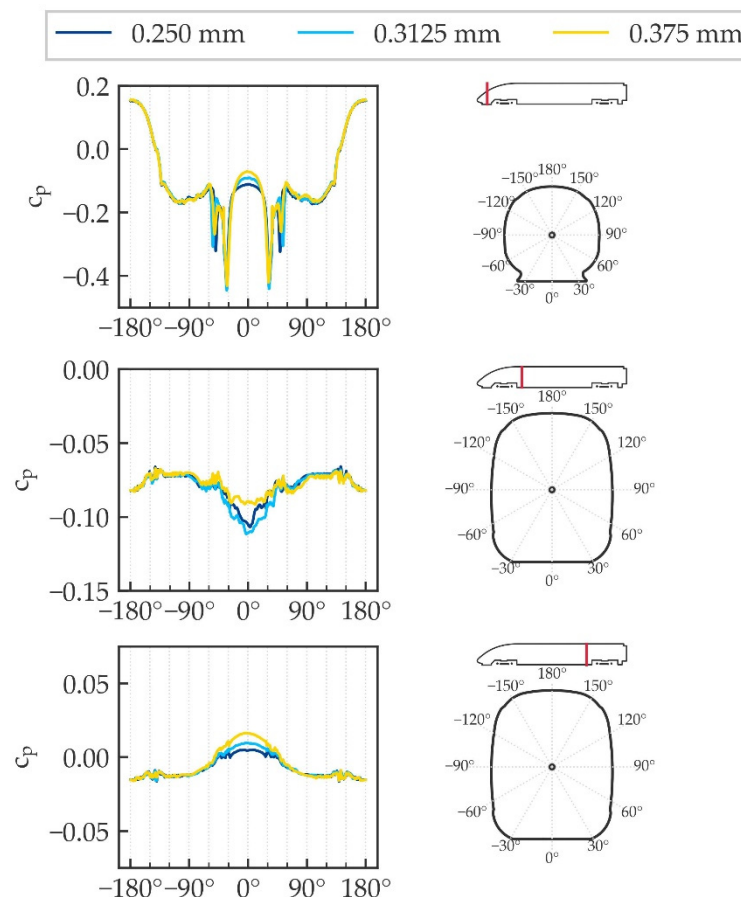


Figure 7. Grid sensitivity of the surface pressures for different sections along the head car.

3. Results

This section is structured as follows: Firstly, the experimental results are presented and discussed focusing on the difference between moving and stationary ground. Afterwards, the pressure tap measurements are used to validate the CFD setup. Differences between the

two simulated ground conditions are highlighted. Finally, the results of the drag reduction due to bogie fairings is compared between wind tunnel measurements and simulation.

3.1. Experimental Results

As the aerodynamic forces on the model support are relevant, the following reported forces and moments are differences between two measurements each: During the first measurement, the train model and support are connected to the underfloor balance. In the second measurement, only the model support is connected to the balance, while the train model is suspended from the wind tunnel’s model manipulator using two steel rods (Figure 4). The forces and moments are normalized according to Equations (7) and (8), with upstream velocity v_∞ , air density ρ , characteristic length $L = 0.15$ m (3 m full-scale) and characteristic area $A = 0.025$ m² (10 m² full-scale).

$$c_i = \frac{F_i}{\frac{1}{2}\rho Av_\infty^2} \tag{7}$$

$$c_{Mi} = \frac{M_i}{\frac{1}{2}\rho ALv_\infty^2} \tag{8}$$

Figure 8 shows mean aerodynamic coefficients for a yaw angle sweep in the range of -20° to 20° measured with moving ground as well as static ground. Mean in this instance refers to the average of the absolute values for both positive and negative yaw angles (Equation (9)).

$$\overline{|c_i(\beta)|} = \frac{1}{2}(|c_i(-\beta)| + |c_i(+\beta)|) \tag{9}$$

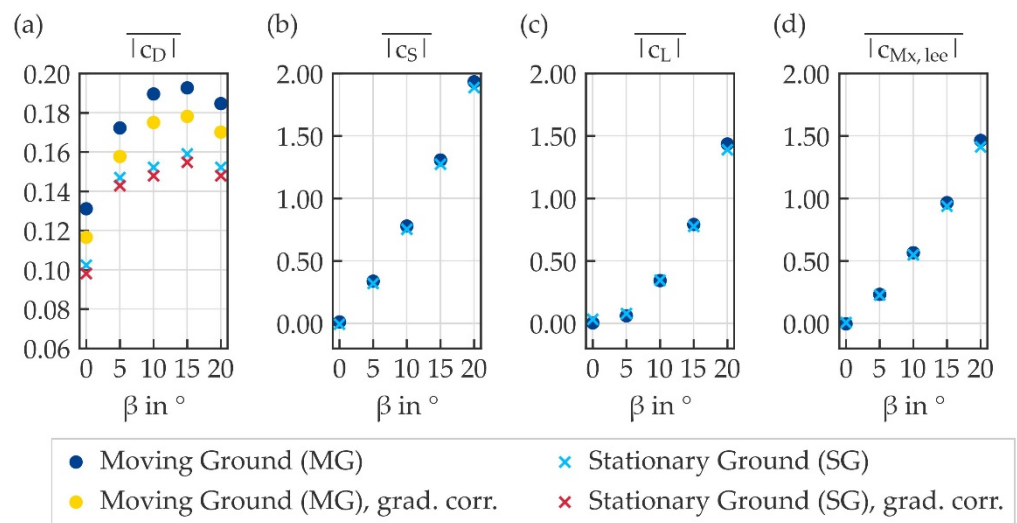


Figure 8. (a) Mean drag coefficient, (b) mean side force coefficient, (c) mean lift coefficient and (d) mean lee rail rolling moment coefficient for yaw angles β between 0° and 20° using moving ground (MG) and stationary ground (SG).

Therefore, small misalignments of the model and wind tunnel turntable are considered. The blockage at 0° yaw is 1.5% and 7.6% at 20° including the downstream body.

For the separate drag datasets marked with the suffix *grad. corr.* (short for gradient correction), the wind tunnel’s static pressure gradient is considered (Figure 8a). This is important for two reasons: Firstly, the pressure gradient is different when using the ground simulation systems, especially at the front of the centerbelt. Secondly, due to the length of the train model, the train’s nose, which is a major contributor to the pressure drag, is close to the front of the centerbelt. The nose pressure drag is therefore directly affected by the changed pressure gradient. The measured pressure gradients (published in [13]) are

interpolated linearly and subsequently integrated over the surface. The resulting virtual drag force coefficients due to the pressure gradients are then subtracted from the measurements.

Figure 8a shows significant differences in drag depending on the ground simulation. At 0° yaw, the drag coefficient using the moving ground is 28% higher than in the static ground measurement (without pressure gradient correction). With the pressure gradient correction, the difference shrinks to 19%. Over the complete yaw angle range, the drag using the moving ground is significantly higher (17% to 28% without correction, 10% to 19% with correction). The rolling moment coefficient around an axis on top of the leese side rail (short: lee rail rolling moment coefficient, $c_{M_x,lee}$) is the main aerodynamic quantity for crosswind safety assessments. As shown in Figure 8d, the lee rail rolling moment is similar using a static or moving ground. It is slightly increased at higher yaw angles using the moving ground, with an increase of 3.6% at 20° yaw. Similar increases in side force coefficient (Figure 8b) and lift coefficient (Figure 8c) indicate that the spatial pressure distribution remains similar. The datasets shown in Figure 8 are available as Supplementary Material Table S1.

The pressure differences at the pressure taps between runs with moving ground and with static ground are plotted in Figure 9 for 0° yaw. As mentioned previously, the static accuracy of the pressure measurement system is ±7 Pa. Thus, for a wind speed of 50 m/s the accuracy of the measured pressure coefficients is around ±0.005. The differences at most pressure taps are small, but three areas with larger differences are highlighted as (1) to (3). Their locations are marked in Figure 10. As expected, they are mainly located on the model’s underbody, especially at the front: (1) on the underside of the nose tip, (2) on the underbody downstream of the cowcatcher and (3) at the rear vertical surface of the front bogie cutout.

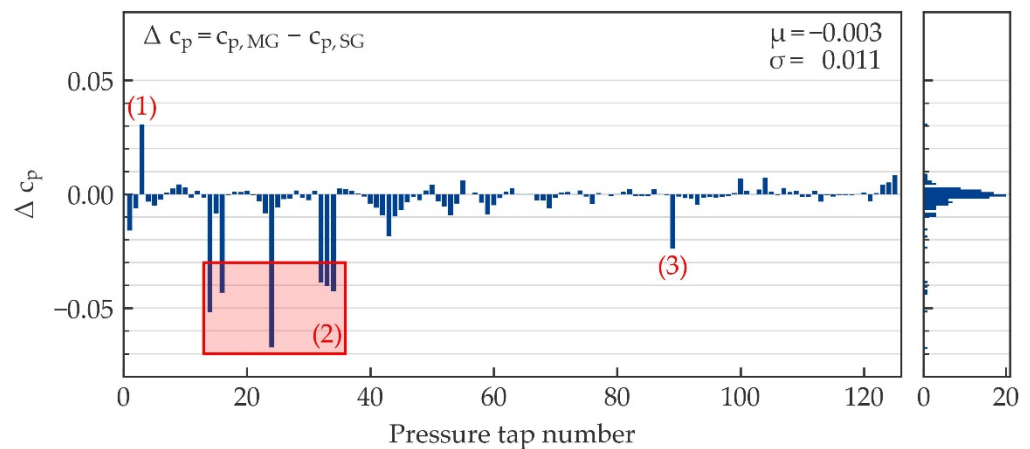


Figure 9. Difference in pressure at pressure taps between moving ground and static ground measurements, main differences numbered (1) to (3).

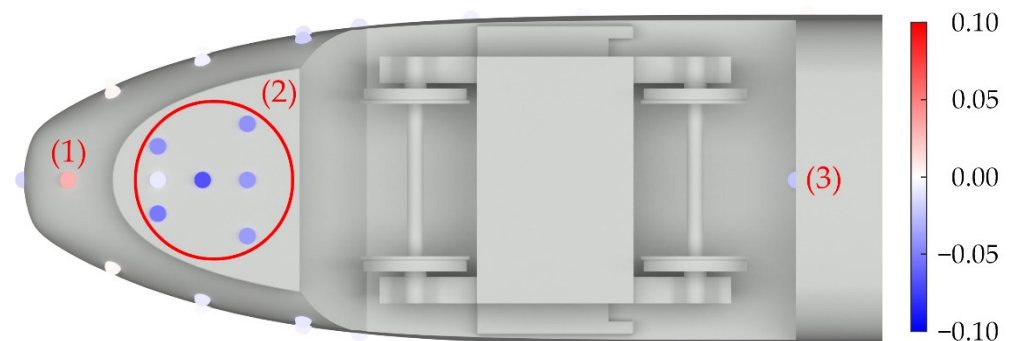


Figure 10. Difference in pressure at pressure taps on underside of train nose between moving ground and static ground measurements.

3.2. CFD Validation

For the validation of the CFD setup, the surface pressure measurements of the moving ground wind tunnel tests are compared to the surface pressures of the idealized CFD simulations (Figure 11). The differences between the full moving ground CFD and moving ground experiment are shown in Figure 11a.

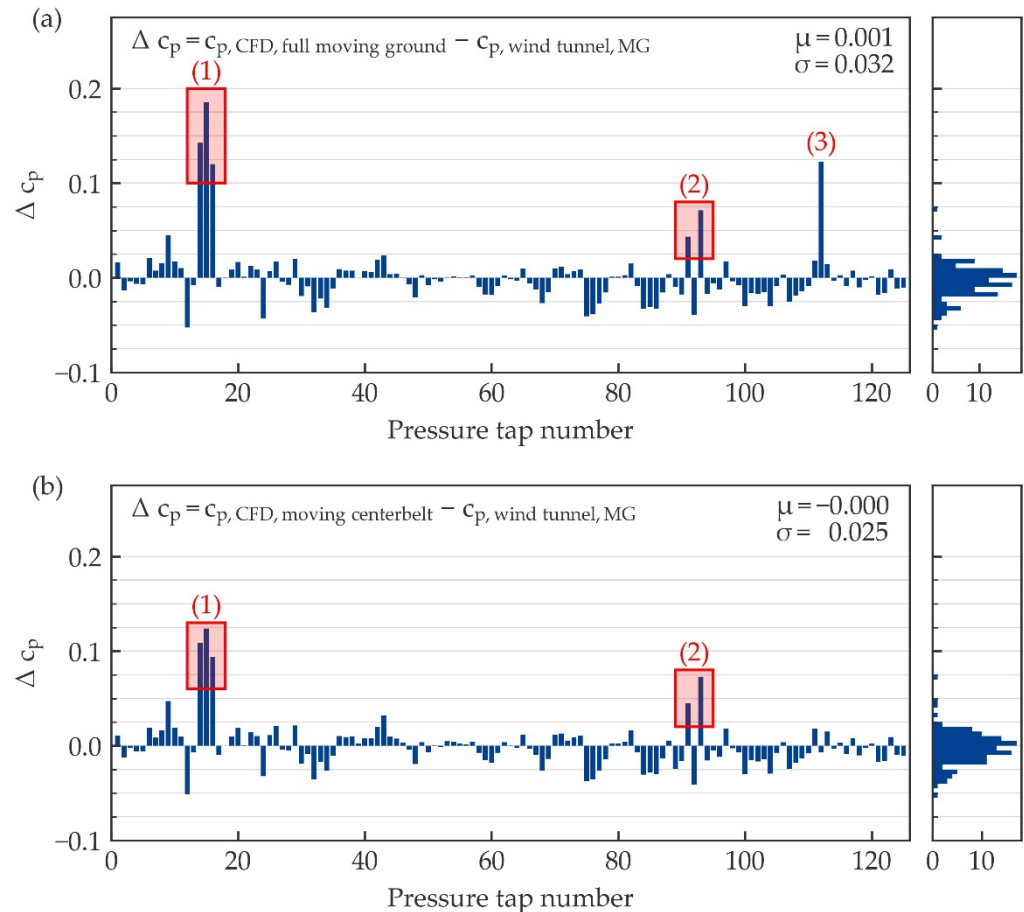


Figure 11. Difference in pressure at pressure taps between CFD simulation and moving ground wind tunnel tests, (a) full moving ground CFD, (b) moving centerbelt CFD.

Most of the pressures agree well, but again three distinct areas of larger deviations can be identified: (1) are the three leftmost pressure taps of region (2) highlighted in Figure 10. As these taps are located in the region of strongest suction and a large pressure gradient in the flow direction is present, more substantial absolute differences compare to other pressure taps are expected. (2) are pressure taps located on the side of the train above the front support crossbeam, which is not part of the idealized simulation setup. Therefore, these two differences can be explained by the simplifications of the idealized setup. (3) is the last pressure tap on the underside of the train, just upstream of the rear bogie cutout.

Switching to the moving centerbelt ground simulation reduces some of the deviations between CFD and experiment (Figure 11b). The differences in area (1) are significantly decreased. Analysis of the surface pressures showed that using the centerbelt configuration, the low pressure region is moved slightly downstream and the low pressure peak is weakened. The deviation of (3) is now insignificant, indicating that the dimensions of the centerbelt affect the rear underbody flow. An additional simulation confirmed that these improvements are due to the dimensions of the centerbelt and not because of its modeled roughness. As expected, the deviations highlighted as (2) are not reduced. These pressure taps are located 128 mm above the ground and thus are not affected by the ground simulation. Overall, wind tunnel measurements and simulations agree

well. The comparison between full moving ground and moving centerbelt simulations have shown that modeling the wind tunnels centerbelt in the simulation is preferable for validation purposes.

3.3. Flow Differences (CFD)

The underbody region upstream of the first bogie has been identified to be dependent on the simulation's ground boundary condition. Figure 12 shows the pressure difference (left column) and velocity magnitude difference (right column) between the simulation using a moving centerbelt and the simulation using a full moving ground for two underbody sections.

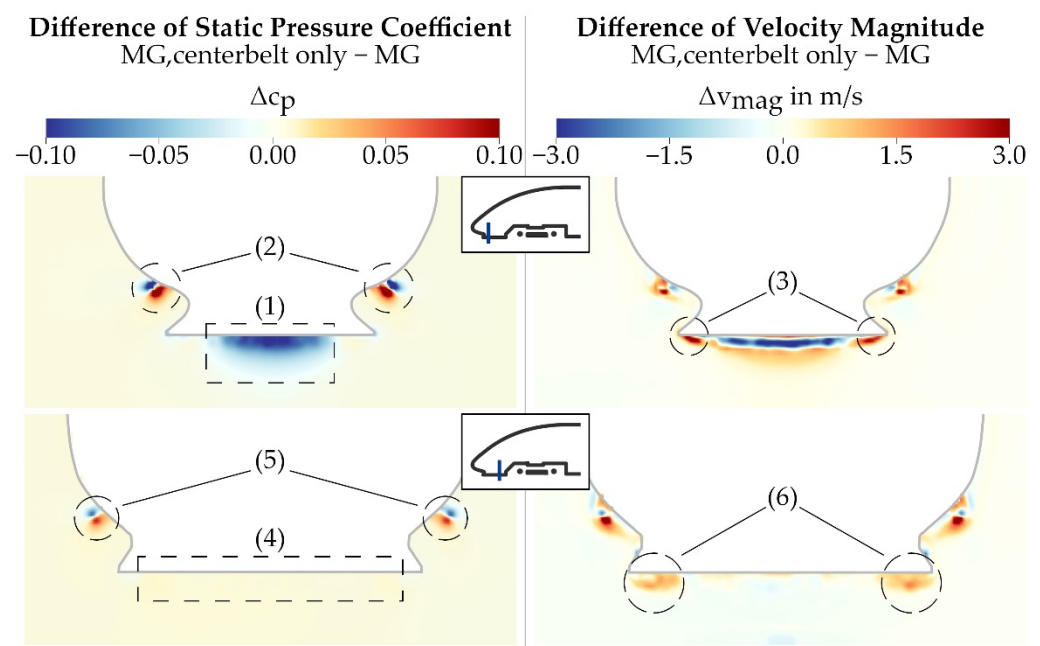


Figure 12. Difference of static pressure and velocity magnitude between moving centerbelt and moving ground simulation for two underbody sections.

The sections are aligned with the lines of three pressure taps on the underside of the train nose (see (2) of Figure 9). Areas of interest are highlighted as (1)–(6). As discussed in the previous section, the pressure due to the flow separation at the cowcatcher is significantly lower for the moving centerbelt case (1). Additionally, the small vortices on the side of the train nose are shifted slightly upwards (2). Further downstream, these vortices interact with the flow separating at the leading edges of the bogie cutouts. Near the edges of the cowcatcher, the lengthwise and crosswise flow velocity is increased (3). In the section just in front of the bogie cavity (second row of Figure 12), the pressure difference on the underside is insignificant (4). The vortex cores either side of the nose are still shifted upwards (5). The flow velocity at the edges of the cowcatcher is slightly higher with an increased velocity towards the center plane (6).

3.4. Bogie Fairings

The drag reductions due to the bogie fairings are shown in Figure 13. Three configurations were tested: Using fairings only at the front bogie, just at the rear bogie and using fairings at both bogies. These configurations were tested in the model scale wind tunnel with static and moving ground conditions. Using CFD, the same configurations were simulated using the fully moving ground as well as the centerbelt moving ground.

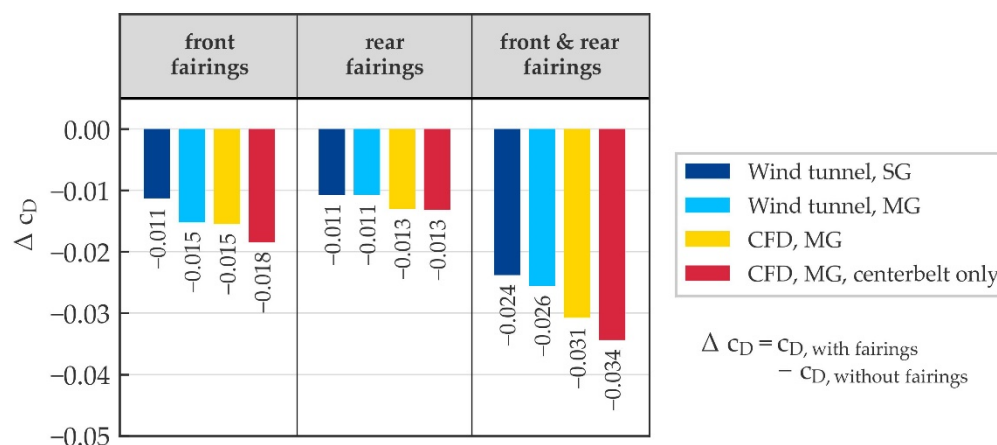


Figure 13. Drag reductions due to bogie fairings, experiment vs. simulation.

Comparing the experimental results, a significant ground simulation effect can be observed: Using the stationary ground, both the front and rear fairings result in a drag reduction of 11 counts. However, using the moving ground, the drag reduction due to the fairings at the front bogie increases to 15 drag counts. Employing fairings at both the front and rear bogie reduces the drag by 24 drag counts using the static ground and 26 drag counts using the moving ground.

Like the moving ground wind tunnel tests, both CFD setups predict a higher drag improvement for the front fairings than for the rear fairings. In case of the full moving ground, this difference amounts to around 2.3 drag counts, whereas the difference is about 5.3 drag counts using only a moving centerbelt. The drag reduction due to the rear fairings is very similar in both cases and slightly larger than in the wind tunnel experiments.

Finally, the CFD simulations overpredict the drag reduction using fairings at both bogies. Compared to the drag reduction of 26 counts measured in the wind tunnel tests, the CFD results are 31 counts and 34 counts for the full moving ground and centerbelt moving ground, respectively. To conclude, both CFD simulations predict a higher drag reduction for the front fairings in line with the moving ground measurements in the wind tunnel. The overall drag reductions are higher in the simulations than in the wind tunnel tests.

4. Discussion

As other studies [5–7] have shown, a moving ground significantly affects the absolute drag. In the wind tunnel tests of this study, the differences of the head car's drag for yaw angles up to 20° were between 10% and 19%, with the maximum difference at 0° yaw. As the static pressure gradient in the test section is dependent on the employed ground simulation techniques, it has to be considered when comparing different measurements. For crosswind investigations concerning the lee rail rolling moment, the effect of the ground simulation is small.

The measurements with different configurations of bogie fairings showed that a moving ground might be important to assess such geometry changes near the ground. Although the absolute drag differences between moving and static ground measurements are fairly small, the measurements on static ground may lead to wrong conclusions: While fairings at the front and rear bogies were valued the same using a static ground, the moving ground measurements showed a stronger drag improvement for the front bogie fairings.

Pressures at the pressure taps coincided well between experiments and simulations. Larger deviations were reduced by switching from a full moving ground to a moving ground section sized according to the wind tunnel's centerbelt. The simulated absolute drag was unaffected by this change, but the drag reductions due to the bogie fairings were increased slightly. Further research to determine the effects of the centerbelt's dimensions might be valuable. Although a good agreement between simulation and experimental

results was achieved using the simplified simulation setup, simulations with the model support geometry are desirable.

Supplementary Materials: The following supporting information can be downloaded at: <https://www.mdpi.com/article/10.3390/fluids7070228/s1>, Table S1: Aerodynamic coefficients for yaw sweep in model scale wind tunnel using moving ground and stationary ground.

Author Contributions: Conceptualization, D.S. and T.K.; methodology, D.W., D.S. and T.K.; software, D.W.; validation, D.W.; formal analysis, D.W.; investigation, D.W. and D.S.; resources, T.K. and A.W.; data curation, D.W.; writing—original draft preparation, D.W.; writing—review and editing, T.K.; visualization, D.W.; supervision, T.K. and A.W.; project administration, D.S.; funding acquisition, A.W. All authors have read and agreed to the published version of the manuscript.

Funding: This research received no external funding.

Institutional Review Board Statement: Not applicable.

Informed Consent Statement: Not applicable.

Data Availability Statement: Not applicable.

Conflicts of Interest: The authors declare no conflict of interest.

References

- Baker, C.J.; Gilbert, T.; Jordan, S. The validation of the use of moving model experiments for the measurement of train aerodynamic parameters in the open air. In Proceedings of the World Congress of Railway Research (WCRR) 2013, Sydney, Australia, 25–28 November 2013.
- Tschepe, J.; Nayeri, C.N.; Paschereit, C.O. Analysis of moving model experiments in a towing tank for aerodynamic drag measurement of high-speed trains. *Exp. Fluids* **2019**, *60*, 98. [[CrossRef](#)]
- Xia, C.; Shan, X.; Yang, Z. Comparison of different ground simulation systems on the flow around a high-speed train. *Proc. Inst. Mech. Eng. Part F J. Rail Rapid Transit* **2017**, *231*, 135–147. [[CrossRef](#)]
- Zhang, J.; Li, J.-j.; Tian, H.-q.; Gao, G.-j.; Sheridan, J. Impact of ground and wheel boundary conditions on numerical simulation of the high-speed train aerodynamic performance. *J. Fluids Struct.* **2016**, *61*, 249–261. [[CrossRef](#)]
- Niu, J.; Wang, Y.; Liu, F.; Li, R. Numerical study on comparison of detailed flow field and aerodynamic performance of bogies of stationary train and moving train. *Veh. Syst. Dyn.* **2020**, *59*, 1844–1866. [[CrossRef](#)]
- Baker, C.J.; Brockie, N.J. Wind tunnel tests to obtain train aerodynamic drag coefficients: Reynolds number and ground simulation effects. *J. Wind Eng. Ind. Aerodyn.* **1991**, *38*, 23–28. [[CrossRef](#)]
- Kwon, H.-B.; Lee, D.-H.; Baek, J.-J. An Experimental Study of Aerodynamic Drag on High-speed Train. *KSME Int. J.* **2000**, *14*, 1267–1275.
- Kwon, H.-B.; Park, Y.-W.; Lee, D.-H.; Kim, M.-S. Wind tunnel experiments on Korean high-speed trains using various ground simulation techniques. *J. Wind Eng. Ind. Aerodyn.* **2001**, *89*, 1179–1195. [[CrossRef](#)]
- Ernst, J.; Falco, M.; Voelker, H.; Arregui, R.; Varela, M.; Heibl, S.; Dittus, H.; Iraklis, A.; Berg, M.; Weinmann, R.; et al. Shift2Rail FINE 1 (Future Improvement for Energy and Noise): D3.1 Energy Baseline, 2018. Available online: https://projects.shift2rail.org/s2r_ipcc_n.aspx?p=FINE%201 (accessed on 23 May 2022).
- Wang, J.; Gao, G.; Li, X.; Liang, X.; Zhang, J. Effect of bogie fairings on the flow behaviours and aerodynamic performance of a high-speed train. *Veh. Syst. Dyn.* **2020**, *58*, 890–910. [[CrossRef](#)]
- Deutsches Institut für Normung e.V. *Railway Applications—Aerodynamics—Part 6: Requirements and Test Procedures for Crosswind Assessment*, German Version EN 14067-6:2018; Beuth Verlag GmbH: Berlin, Germany, 2018.
- Tschepe, J.; Nayeri, C.N.; Paschereit, C.O. On the influence of Reynolds number and ground conditions on the scaling of the aerodynamic drag of trains. *J. Wind Eng. Ind. Aerodyn.* **2021**, *213*, 104594. [[CrossRef](#)]
- Wittmeier, F. The Recent Upgrade of the Model Scale Wind Tunnel of University of Stuttgart. *SAE Int. J. Passeng. Cars Mech. Syst.* **2017**, *10*, 203–213. [[CrossRef](#)]
- Krüger, T.; Kusumaatmaja, H.; Kuzmin, A.; Shardt, O.; Silva, G.; Viggien, E.M. *The Lattice Boltzmann Method: Principles and Practice*; Springer International Publishing: Cham, Switzerland, 2017.
- Kotapati, R.; Keating, A.; Kandasamy, S.; Duncan, B.; Shock, R.; Chen, H. The Lattice-Boltzmann-VLES Method for Automotive Fluid Dynamics Simulation, a Review. In *SAE Technical Paper*; 2009-26-0057; Springer: Berlin/Heidelberg, Germany, 2009. [[CrossRef](#)]
- Chen, H.; Kandasamy, S.; Orszag, S.; Shock, R.; Succi, S.; Yakhot, V. Extended Boltzmann Kinetic Equation for Turbulent Flows. *Science* **2003**, *301*, 633–636. [[CrossRef](#)] [[PubMed](#)]
- Pervaiz, M.M.; Teixeira, C.M. Two equation turbulence modeling with the lattice-Boltzmann method. *ASME Publ. PVP* **1999**, *397*, 15–24.